Electrical properties of a $LiTaO_3$ single crystal

D. C. Sinclair and A. R. West
University of Aberdeen, Department of Chemistry, Meston Walk, Aberdeen AB9 2UE, United Kingdom
(Received 7 September 1988)

$LiTaO_3$ is both a modest conductor of Li^+ ions and electrons at high temperatures and a ferroelectric. From ac-impedance data recorded over a wide temperature (500–700 °C) and frequency (30 mHz–1 MHz) range, it was possible to measure the following with the crystal **c** axis oriented parallel to the electric field: the charge polarization associated with the ferroelectric domains, the intrinsic polarization—which is high but not ferroelectric—of the crystal structure, the resistance associated with domain reorientation, and the resistance due to lithium-ion migration. The correct choice of equivalent circuit is crucial to the determination of these parameters. With the crystal **c** axis oriented perpendicular to the electric field, a much simpler response was seen. The capacitance values are small, have very little temperature dependence, and show no signs of ferroelectricity. Also the crystal is a modest electronic conductor at high temperatures, 500–700 °C, in this orientation. These results indicate the potential of the ac-impedance technique for probing the electrical properties of ferroelectric materials; some of the disadvantages associated with using fixed-frequency dielectric loss measurements are discussed.

INTRODUCTION

$LiTaO_3$ is a ferroelectric material with a Curie point around 600 °C, the precise value depending on the [Li]-to-[Ta] ratio.[1] An ac-impedance study of ceramic samples[2] showed, in addition to the ferroelectric properties, a modest level of conductivity at high temperatures which was attributed to the motion of Li^+ ions, at least in the off-stoichiometric materials. This study showed the potential usefulness of ac impedance for characterizing ferroelectric materials; however, the need for measurements on single-crystal samples to determine the importance of crystal orientation effects, to separate bulk and grain boundary resistances, and to better separate the conduction and ferroelectric phenomena was clearly identified.

ac-impedance measurements provide a means of obtaining a more complete electrical characterization of materials than would be obtained from, for example, tanδ or dielectric loss measurements, especially if these latter are restricted to single-frequency measurements. For impedance analyses, it is crucial to have not only an appropriate equivalent circuit with which to analyze the data, but also a circuit which provides a realistic representation of the processes occurring inside the sample. Here we report ac-impedance results on single-crystal $LiTaO_3$ in two crystallographic orientations, parallel to and perpendicular to the **c** axis, and show, particularly by attention to the nature of the capacitances and their temperature dependence, how it is possible to arrive at an equivalent circuit which both fits the data and can be related to electrical phenomena occuring in the sample. Thus for a particular data set, it is usually possible to find at least two equivalent circuits which can be matched to the data and additional information is required to help decide which of the circuits is most appropriate.

The equivalent circuit deduced for $LiTaO_3$ allows us to determine its conductivity and also, for the crystal **c** axis oriented parallel to the electric field, to separate and measure the resistance and capacitance components of the ferroelectric polarization process. Domain reversal can be followed as a function of temperature, by means of a macroscopic resistance parameter and the intrinsic permittivity of the sample can be separated from that associated with cooperative ordering in the domains.

Data measured as complex impedances may be converted to any of three other formalisms, admittance, Y^*; permittivity, ϵ^*; or electric modulus, M^*.[3] These formalisms are interrelated by

$$M^* = j\omega C_0 Z^*, \quad M^* = (\epsilon^*)^{-1},$$
$$Z^* = (Y^*)^{-1}, \quad Y^* = j\omega C_0 \epsilon^*,$$

where ω is the angular frequency, $2\pi f$. Results may be presented in various ways, e.g., as complex plane plots (real versus imaginary, usually on linear scales) or as spectroscopic plots (real and/or imaginary against frequency). Sometimes, three-dimensional plots are used with real and imaginary components and frequency as the axes.[4] There are no hard and fast rules as to which type of plot is most appropriate; rather this depends on the nature of the material under study and the particular information that is required.

EXPERIMENTAL

The single crystal of $LiTaO_3$ used in this study was provided by C. Carter of Plessey in the form of a disk, 0.12 mm thick and 14 mm in diameter. The crystallographic **c** direction was perpendicular to the disc faces. For impedance measurement with the electric field parallel to *c*, gold electrodes were evaporated onto opposite crystal faces and impedance measurements made with a two-terminal electrode configuration. The crystal and electrodes were attached, via organogold paste, to the Pt

leads of a conductivity jig and placed inside a tube furnace whose temperature was controlled and measured to within 3°. For impedance measurements with the electric field perpendicular to c, gold paste electrodes were attached to opposite edges of an approximately rectangular crystal fragment.

For both crystal orientations, the blank parallel capacitance of the conductivity jig, without the crystal, was measured and appropriate corrections made to the experimental data. The leak resistance of the jig was found to be large, >100 MΩ, and was much greater than that of the crystal at all temperatures studied. The resistance of the electrode leads was <1 Ω, as shown by shorting out the crystal and was too small to influence the impedance data.

For most of the impedance measurements, a Solartron 1250/1286 FRA setup was used, covering the frequency range 30 mHz to 65 kHz with a nominal applied voltage of 100 mV. Some data were recorded using a Solartron 1260 Impedance Analyzer which enabled measuring frequencies up to 1 MHz to be used; results from the two sets of instruments were comparable. Prior to each set of measurements, the jig was allowed to equilibrate at the temperature of the furnace for 45 min. Measurements were made, isothermally, on both heating and cooling cycles and were found to be reproducible with no hysteresis. The temperature range covered was 500–700 °C; all measurements were made in air.

The composition of the $LiTaO_3$ crystal is an off-stoichiometric, Ta_2O_5-rich composition. The Curie temperature that has been deduced from our studies 590 °C is consistent with a composition, $Li_{0.95}Ta_{1.01}O_3$ (Ref. 1) in which departure from the $LiTaO_3$ stoichiometry is accommodated by lithium-ion vacancies associated with the substitution mechanism, $5\ Li^+ \rightleftharpoons Ta^{5+}$. The Curie temperature varies markedly with composition[1] and provides an accurate measure of composition.

RESULTS

We chose to begin presentation of the ac data for $LiTaO_3$, obtained in the ferroelectric orientation, i.e., with the electric field parallel to c, using the permittivity formalism since this gives a convenient means of extracting capacitance values. Results are shown in Fig. 1 for the real part ϵ' of the permittivity as a function of frequency for four temperatures. The data show an approximately frequency-independent region above about 100 kHz and a second frequency-independent region around 1 kHz. At lower frequencies, the permittivity rises markedly. Data were recorded for many other temperatures in the range 500–700 °C and all had the same general appearance as those shown in Fig. 1.

The first step in interpreting data such as those of Fig. 1 is to extract capacitance values for the two frequency-independent regions, convert them to permittivities using the relation $\epsilon' = C/C_0$, where C_0 is the vacuum capacitance of the cell without the sample, and plot the ϵ' data against temperature, Fig. 2(a). Both data sets pass through a maximum at the Curie temperature, 590 °C, but only one, corresponding to the lower frequency capacitance, C_l, gives a linear Curie-Weiss plot of reciprocal permittivity (or reciprocal capacitance) against temperature, Fig. 2(b). It seems likely, therefore, that C_l represents directly the polarization associated with the ferroelectric domains but that C_h is a composite capacitance without a well-defined temperature dependence.

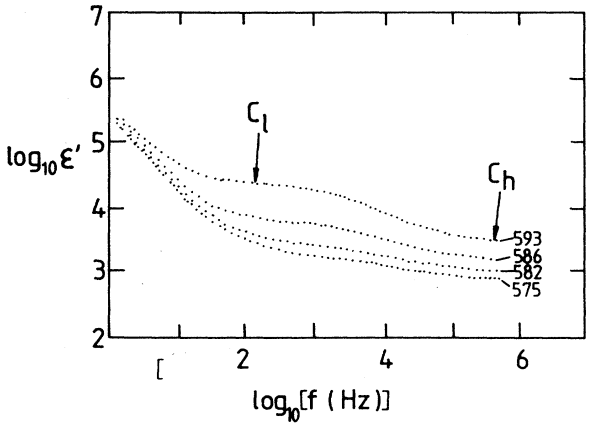

FIG. 1. Permittivity data for four temperatures.

The next stage is to find an appropriate equivalent circuit to represent the data. Three possible circuits which merit consideration are shown in Figs. 3(a)–3(c). The first two could be appropriate to dielectric or ferroelectric

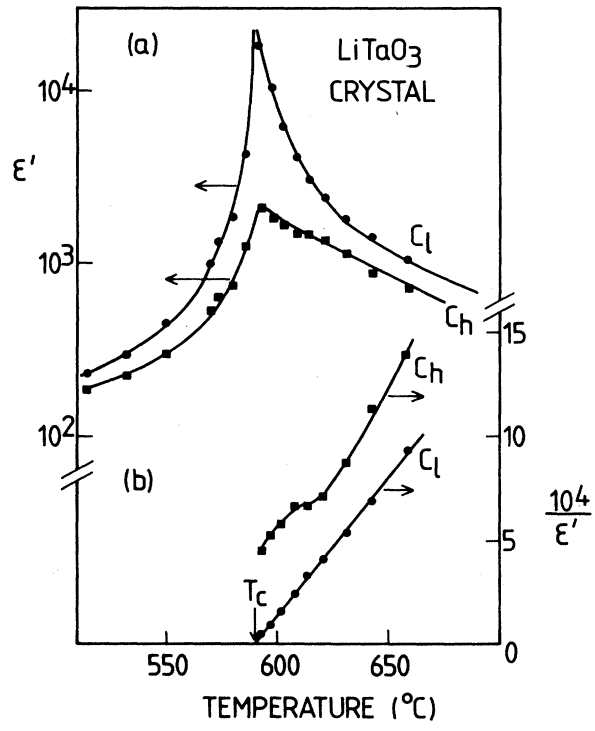

FIG. 2. Permittivity data plotted against temperature in (a) and as Curie-Weiss plots in (b).

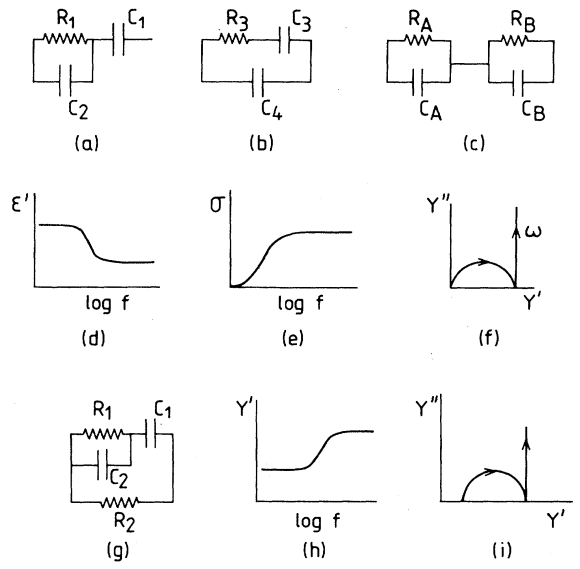

FIG. 3. (a)–(c) plausible equivalent circuits with (d)–(f) their permittivity and conductivity plots. (g) circuit chosen for $LiTaO_3$ with (h) and (i) its conductivity response.

materials without residual or leakage conductivity. The third is commonly used to represent series phenomena in heterogeneous conducting materials and in which, parallel RC elements are used to represent for instance bulk, grain boundary, surface layer, or electrode effects. All three circuits show low- and high-frequency plateaus in a plot of permittivity against frequency, as shown schematically in Fig. 3(d) and cannot be distinguished purely from the shape of this plot. The capacitances associated with the plateaux in (d) can be evaluated from the overall impedance-admittance equations of the circuits and have the values listed in Table I.

The experimental data were compared with the ac response of each of these three circuits and capacitance values extracted; note that at this stage, we are excluding from consideration the low-frequency, monotonic rise in permittivity seen in Fig. 1. For circuit (a), capacitance C_1 corresponds directly to the experimental C_l value

TABLE. I. Limiting, frequency-independent permittivities and their associated capacitances for the circuits shown in Fig. 3.

Circuit	$\epsilon'(\omega\rightarrow 0)$	$\epsilon'(\omega\rightarrow\infty)$
(a)	$\frac{C_1}{C_0}$	$\frac{C_1C_2}{C_0(C_1+C_2)}$
(b)	$\frac{C_3+C_4}{C_0}$	$\frac{C_4}{C_0}$
(c)	$\frac{C_AR_A^2+C_BR_B^2}{C_0(R_A+R_B)^2}$	$\frac{C_AC_B}{C_0(C_A+C_B)}$

(Table I) and therefore shows the Curie-Weiss behavior of Figs. 2(b) and 4. Capacitance C_2 extracted from the high-frequency plateau is quite different and shows two temperature-independent regions separated by a dispersion over a range of temperatures up to and including the Curie temperature, Fig. 4. For circuits (b) and (c), neither of the two capacitances showed either Curie-Weiss behavior or temperature-independent behavior. From this, it is concluded that circuits (b) and (c) do not offer a physical representation of the permittivity behavior of $LiTaO_3$. By contrast, circuit (a) may be related directly to physical properties of the sample since the associated capacitance values have a well-characterized temperature dependence. Circuit (a) is therefore used as the starting point for further analysis.

Turning now to the resistive component(s) of the equivalent circuit, it is expected that the conductivity (conductivity is equivalent to the real part of the admittance Y') would, ideally, show the behavior of Fig. 3(e), with a frequency-independent plateau at high frequencies. Alternatively, the complex admittance plane should show a semicircle passing through the origin at low frequencies and a high-frequency spike, as in Fig. 3(f). The experimental data, shown in Fig. 5, are however, more complex. They show parts of two frequency-independent regions in conductivity against frequency, (a) and (b), although clear evidence for the higher frequency plateau is seen only in data close to the Curie point. At other temperatures, the high-frequency plateau is at frequencies outside the measuring range. The existence of the high-frequency plateau in (a) and (b) is seen more clearly in the

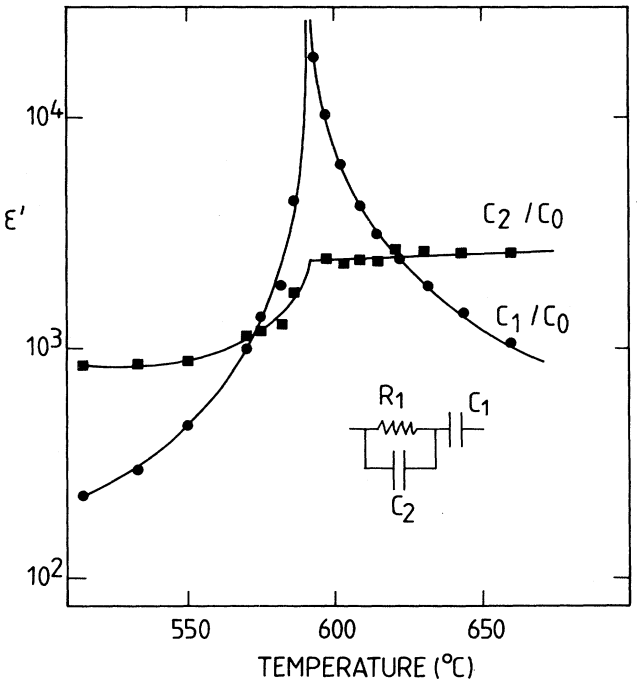

FIG. 4. Capacitance values extracted with Fig. 3(g) as the equivalent circuit.

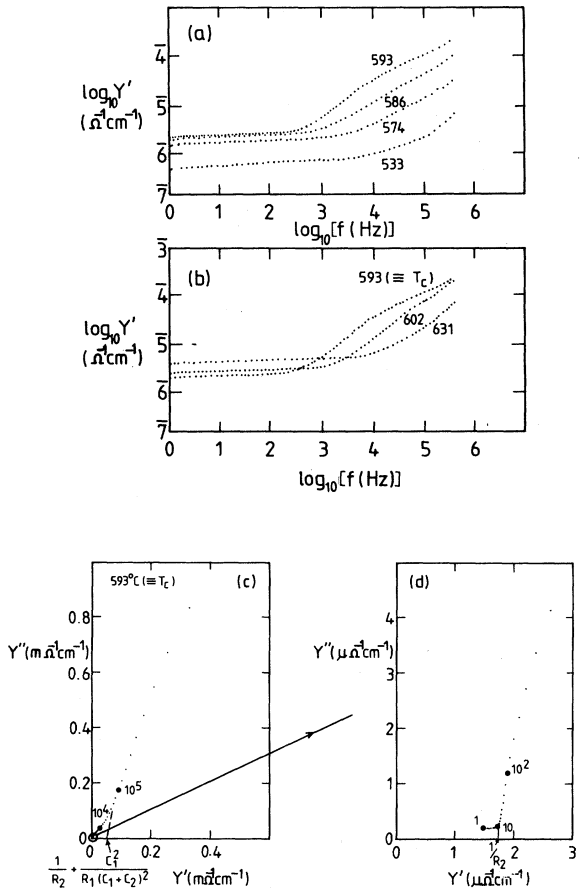

FIG. 5. Experimental data in the form of (a) and (b), frequency-dependent conductivities, and (c) and (d), complex admittances.

complex admittance plane (c). A nonzero low-frequency intercept for the semicircle in the complex admittance plane, (c) and (d), corresponds to the low-frequency plateau in (a) and (b) whereas the high-frequency intercept of the rather poorly defined semicircle in (c) corresponds to the high-frequency plateau in (a) and (b).

Clearly, the equivalent circuit must contain two resistances and modification to Fig. 3(a) is required. Since the additional resistance appears to provide a dc pathway through the sample, it is appropriate to put it in parallel with the dielectric component of the sample, yielding the circuit shown in Fig. 3(g). From the equation for the complex admittance of this circuit, resistance values may be extracted as indicated in Table II and Figs. 5(c) and 5(d).

Experimental resistance values obtained from the admittance plots are presented in Arrhenius format in Fig. 6. Resistance R_2 is linear over the whole temperature range studied, with an activation energy of 1.27±0.01 eV. Resistance R_1 is essentially linear well below T_C, with an activation energy of about 5 eV, but shows increasing curvature as T_C is approached, terminating with an abrupt decrease at T_C; at temperatures above the Curie point, it was not possible to obtain an accurate estimate of R_1 but it appears to be nonzero, at least for a short range of temperatures.

TABLE II. Limiting conductivities, Y' for the circuit in Fig. 3(g). The complex admittance, Y^*, for this circuit is given by $Y^*=\{[1/(1/R_1+jwC_2)]+(1/jwC_1)\}^{-1}+1/R_2$.

$Y'(\omega\rightarrow 0)$	$Y'(\omega\rightarrow\infty)$
$\frac{1}{R_2}$	$\frac{C_1^2}{R_1(C_1+C_2)^2}+\frac{1}{R_2}$

In order to ascertain whether R_2 is associated with migration of lithium ions or electrons, information was sought in the low-frequency region of the ac response. Specifically, the low-frequency admittance data were seen to terminate not at the nonzero intercept on the real axis, but to give an additional very low-frequency semicircle which appeared to extend towards the origin. Only a small part of this low-frequency semicircle is seen in Fig. 5(d), at frequencies below ~10 Hz, but at higher temperatures, as R_2 decreases, more of this semicircle was seen.

This effect is also shown, more clearly perhaps, in the complex impedance representation, Fig. 7, in which the low-frequency response appears as an inclined spike. Such a spike is characteristic of a blocking double-layer capacitance, whose magnitude may be estimated from any position on the spike using the equation $Z''=1/2\pi fC$. Values of about 2 μF are obtained which

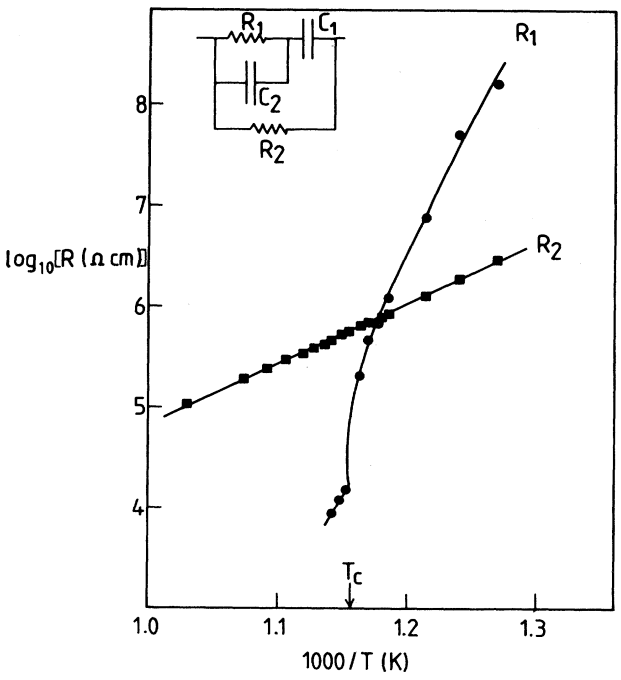

FIG. 6. Arrhenius plots for the resistances R_1 and R_2.

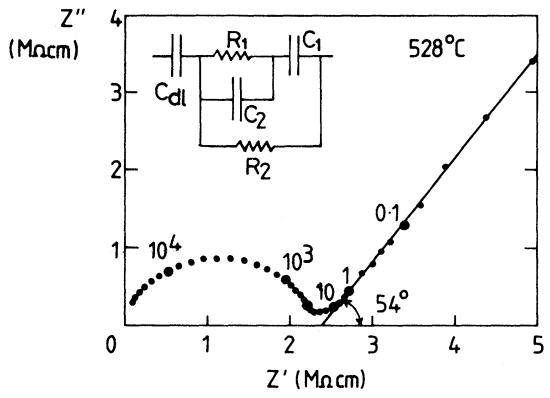

FIG. 7. Complex impedance plot showing a low-frequency "electrode spike."

are typical of those expected for the blocking of ionic charge carriers at the metal-sample interface. It is concluded that the current carriers are, therefore, lithium ions rather than electrons. In order to represent the blocking capacitance, it is necessary to add a series capacitance C_{d1} to the circuit in Fig. 3(g), as shown in Fig. 7.

Impedance measurements made in the nonferroelectric orientation, i.e., with the electric field perpendicular to c, gave a much simpler response. There was no evidence of the resistance R_1 and capacitance C_1 attributed to the ferroelectric domains. Instead, the crystal appeared to be a very modest electronic conductor with a small, temperature-independent bulk capacitance, $C_\perp$. Over the temperature range 500–700 °C, the capacitance value was less than 10 pF/cm; the measured capacitance values of the jig with and without the crystal were comparable and hence the crystal bulk capacitance could not be determined accurately. Such behavior is consistent with that reported by Ballman *et al.*[5]

Resistance values were obtained from the complex impedance plane plots; a typical one is shown in Fig. 8. The data show the low-frequency part of a semicircle, shown dashed, whose intercept on the Z' axis gives the resistance $R_\perp$. At lower frequencies, < 10 Hz, a residual tail is seen in the impedance data but this does not have the character of the electrode spike seen in Fig. 7.

These results for $R_\perp$ and $C_\perp$ are consistent with a simple equivalent circuit composed of a parallel RC element, as shown in Fig. 9. An Arrhenius plot of the $R_\perp$ data is given in Fig. 9; it shows a slight change in slope at T_C with linear regions to either side.

It is very likely that $R_\perp$ corresponds to an electronic resistance which, in this crystal orientation, must be much less than the resistance due to lithium-ion motion. If, instead, $R_\perp$ were due to an ionic resistance, a clearly defined electrode spike would be seen in the impedance plots, Fig. 8: e.g., at a frequency of 0.15 Hz and assuming a double-layer capacitance of 1 μF, the impedance spike should have a Z'' value of around 1 MΩ. As it is, the experimental Z'' value at this frequency is only around 1 kΩ.

On comparing Figs. 6 and 9, the magnitude of $R_\perp$ is about a decade smaller than that of R_2. This shows that parallel to c, lithium-ion conduction predominates, but that perpendicular to c, a higher level of electronic conduction predominates. The electronic conductivity of the crystal must, therefore, show considerable anisotropy. We are unable to comment on whether the Li^+ ion conductivity is isotropic or anistropic.

DISCUSSION

It has been shown that, in the ferroelectric orientation, the electrical properties of a $LiTaO_3$ single crystal can be referred to an ideal equivalent circuit composed of two resistors and two capacitors, Fig. 3(g). Furthermore, it has been shown that other plausible equivalent circuits, based on Figs. 3(b) and 3(c), for the dielectric component of the ac response, do not yield physically significant capacitance parameters. This is because the nature of the temperature dependence of their component C values, Table I, indicates that these are composite parameters

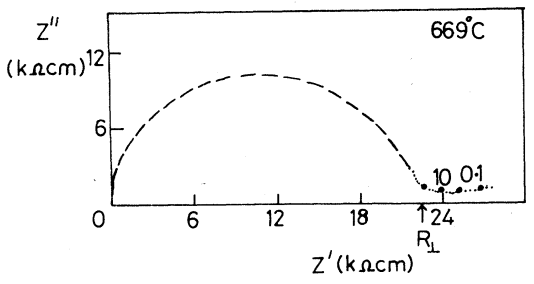

FIG. 8. Complex impedance plot for the nonferroelectric orientation.

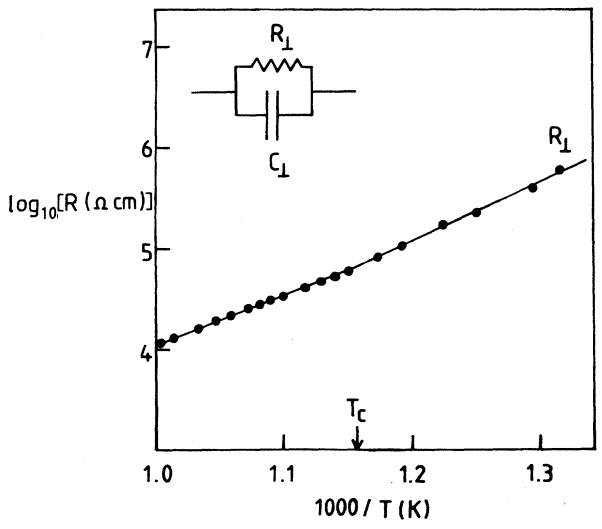

FIG. 9. Arrhenius plot of the electronic resistance in the nonferroelectric orientation.

which cannot be directly related to the properties of the sample. The well-behaved temperature dependence of the C parameters for circuits (a) and (g) has been commented on above: one capacitance shows an ideal Curie-Weiss response and the other shows a discontinuity at T_C. In addition, the R values extracted from circuit Fig. 3(g) and given in Fig. 6, are also well characterized: one resistance shows linear Arrhenius behavior and the other shows a discontinuity at T_C. This again shows that circuit (g) is realistic. In some cases, the wrong choice of equivalent circuit could give rise to nonlinear Arrhenius plots of the extracted R values. This effect is to be discussed more fully elsewhere.[6]

Let us consider now the components of the proposed equivalent circuit, Fig. 3(g), in some detail and discuss their significance. Capacitance C_1 is clearly that associated with the ferroelectric domains. It passes through a sharp maximum at T_C, shows very good Curie-Weiss behavior extrapolating to the Curie temperature, and must be associated with the net polarization of the domains. This domain polarization is reversible, at least partially, under the influence of a small applied electric field, otherwise it would not exhibit such large capacitance values. Domain reversal is easiest in the region of the Curie point, as evidenced by the maximum in C_1 at this temperature. Well below the Curie point, the permittivity of the domains is much reduced because they are essentially fixed in their orientation and cannot be reversed at the small applied voltages used in the impedance measurements. Above T_C, the domains break up into smaller clusters and the amount of correlated polarization that is possible decreases.

Resistance R_1 is in series with the ferroelectric capacitance and must be the resistance associated with domain reversal. Its activation energy ~ 5 eV is much higher than that which is usually ever measured experimentally for conduction by either ions or electrons. It is attributed to the reversal in polarization of complete domains. Thus, while reversal of the individual atomic displacements is likely to have a small or zero activation energy, in R_1 we are measuring the cooperative displacement of a large number of atoms; this is a much more difficult process. The mechanism of this domain reversal is not obtained from these results, i.e., whether it involves complete domain reversal or proceeds by domain-wall migration. The marked temperature dependence of R_1, Fig. 6, also correlates with the rapid changes in C_1: at temperatures well below T_C, the resistance to domain reversal is so large that domain reversal does not occur to any large extent and therefore, the associated capacitance value C_1 is small. R_1 undergoes a rapid decrease at T_C; this is consistent with the breakup of domains as the temperature is increased to T_C and above. There appears to be a small residual R_1 above T_C; this could be associated with the presence of local regions or clusters of ferroelectric polarization.

Capacitance C_2 is not ferroelectric but it is very large and increases markedly on passing through the Curie temperature, Fig. 4. It is attributed to the polarization of the individual lattice components, specifically, the individual Li and Ta ions within the octahedral (Ta) or distorted octahedral (Li) coordination provided by their surrounding oxide ions. This capacitance provides a measure of the small, individual atomic displacements which, when linked cooperatively, give rise to the ferroelectric domains. The increase in polarization on passing through T_C may be due to the removal of crystallographic constraints associated with the existence of cooperative displacements within the noncentric, polar domains at temperatures below T_C. Since the ferroelectric-paraelectric transition has strong second-order character, the polarization of the individual dipoles starts to increase at temperatures well below T_C and is essentially optimized when the Curie temperature is reached. This is reflected in the smooth increase in C_2 as the temperature is increased to T_C.

Resistance R_2 is associated with long-range migration of Li^+ ions through the crystal. Its activation energy 1.27 eV is quite large but is typical of that for stoichiometric crystals with few defects and only a modest degree of ionic conductivity. The crystal structure of $LiTaO_3$ may be described ideally as an hcp array of oxide ions with $\frac{2}{3}$ of the octahedral sites occupied by cations in ordered fashion.[7] These occupied octahedral sites share faces in Li/Ta pairs and cation-repulsion effects cause Li to be displaced away from an adjacent Ta towards three of its coordinated oxide ions. The high value of C_2 may be associated with ready displacement of Li to an adjacent octahedral site on the other side of these three coordinated oxygens.

CONCLUSIONS

These results represent a significant advance over those obtainable by conventional dielectric loss or tanδ measurements, mainly because they enable the fundamental processes occurring in this ferroelectric material to be separated and measured. The impedance technique offers a ready means of monitoring domain reorientation effects and the results obtained should complement those obtained by dc-polarization techniques. For the first time, it has been possible to separate the local and cooperative displacements which contribute to dielectric and ferroelectric polarizations.

Finally, it should be noted that a complete and accurate representation of the ac response of ferroelectric materials is likely to require the use of dispersive elements in the equivalent circuit, such has been suggested and used previously,[8,9] rather than single-valued resistances and capacitances.

ACKNOWLEDGMENTS

D.C.S thanks the Science and Engineering Research Council for support. A.R.W. thanks the Royal Society of Edinburgh for support.

APPENDIX: FIXED-FREQUENCY PERMITTIVITIES AND CURIE-WEISS PLOTS

In the above, we have concentrated on showing the most appropriate way to analyze ac data such that a

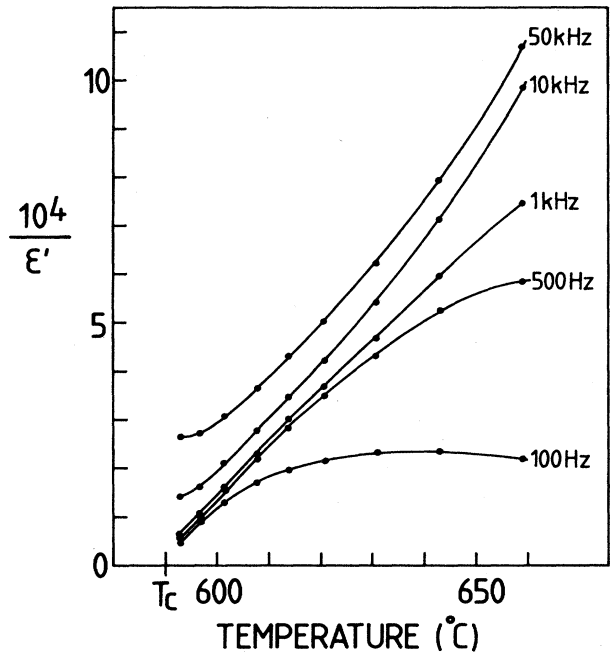

FIG. 10. Curie-Weiss plots from fixed-frequency permittivity data.

physical interpretation of the results may be obtained. There are various other ways of analyzing such data, some of which may give results that are misleading or incorrect. Here, some of the pitfalls associated with using fixed-frequency permittivity data are discussed. To illustrate this, fixed-frequency permittivity values have been extracted from our variable-frequency data sets.

Very commonly, data for ϵ' are obtained at a single frequency only, often 1 kHz, and then plotted either directly against temperature or as Curie-Weiss plots of reciprocal permittivity against temperature. Curie-Weiss plots are shown in Fig. 10 at five fixed frequencies using the experimental data for $LiTaO_3$. The 1 kHz plot is linear over most of the temperature range but at both higher and lower frequencies, gross departures from linearity occur. In this particular case, 1 kHz data could be used as a reasonably accurate representation of the permittivity of the domains, although the intercept of the extrapolated data misses the Curie temperature by a few degrees. This linearity is a fortuitous coincidence, however, and there is no reason to expect that 1 kHz data should be well-behaved generally.

The deviations from linearity in Fig. 10 can all be explained satisfactorily by referring to Fig. 1. At lower frequencies and higher temperatures, e.g., $>600\,^{\circ}C$ for 100 Hz, a downward deviation occurs in Fig. 10, reflecting an overestimate of the ϵ' value. This arises because, in this region, ϵ' is affected by electrode polarization associated with lithium-ion migration and which is responsible for the monotonic rise in ϵ' seen at low frequencies in Fig. 1. This is also the same effect that is responsible for the low-frequency spike in the impedance plots, Fig. 7.

At higher frequencies an upward departure from Curie-Weiss response occurs, e.g., for 10 kHz. This is because the permittivity at this frequency does not correspond to the low-frequency plateau of Fig. 1 but is instead on the dispersion towards the high-frequency plateau value.

[1]Y. Fujino, H. Tsuya, and K. Sugibuchi, Ferroelectrics **2**, 113 (1971).
[2]A. Huanosta and A. R. West, J. Appl. Phys. **61**, 5386 (1987).
[3]I. M. Hodge, M. D. Ingram, and A. R. West, J. Electroanal. Chem. **74**, 125 (1976).
[4]*Impedance Spectroscopy*, edited by J. Ross Macdonald (Wiley, New York, 1987).
[5]A. A. Ballman, H. J. Levinstein, C. D. Capio, and H. Brown, J. Am. Ceram. Soc. **50**, 657 (1967).
[6]D. C. Sinclair, J. T. S. Irvine, and A. R. West (unpublished).
[7]S. C. Abrahams, E. Buehler, W. C. Hamilton, and S. J. Laplaca, J. Phys. Chem. Solids **34**, 521 (1973).
[8]D. P. Almond and A. R. West, Solid State Ionics **11**, 57 (1983).
[9]A. K. Jonscher, *Dielectric Relaxation in Solids* (Chelsea Dielectrics, London, 1983).